



## OPEN ACCESS

## EDITED BY

Nagesh Kolishetti,  
Florida International University,  
United States

## REVIEWED BY

Iram Maqsood,  
University of Maryland, United States  
Wei Shao,  
Westlake University, China  
Prajesh Prajapati,  
National Forensic Sciences University,  
India

## \*CORRESPONDENCE

John B. Cooper,  
✉ jcooper@odu.edu

RECEIVED 31 July 2023

ACCEPTED 25 August 2023

PUBLISHED 12 September 2023

## CITATION

Butler MR, Hrnčirova J, Jacot TA, Dutta S,  
Clark MR, Doncel GF and Cooper JB  
(2023), Detection and quantification of  
antiviral drug tenofovir using silver  
nanoparticles and surface enhanced  
Raman spectroscopy (SERS) with spatially  
resolved hotspot selection.  
*Front. Nanotechnol.* 5:1270474.  
doi: 10.3389/fnano.2023.1270474

## COPYRIGHT

© 2023 Butler, Hrnčirova, Jacot, Dutta,  
Clark, Doncel and Cooper. This is an  
open-access article distributed under the  
terms of the [Creative Commons  
Attribution License \(CC BY\)](https://creativecommons.org/licenses/by/4.0/). The use,  
distribution or reproduction in other  
forums is permitted, provided the original  
author(s) and the copyright owner(s) are  
credited and that the original publication  
in this journal is cited, in accordance with  
accepted academic practice. No use,  
distribution or reproduction is permitted  
which does not comply with these terms.

# Detection and quantification of antiviral drug tenofovir using silver nanoparticles and surface enhanced Raman spectroscopy (SERS) with spatially resolved hotspot selection

Marguerite R. Butler<sup>1</sup>, Jana Hrnčirova<sup>1,2</sup>, Terry A. Jacot<sup>3</sup>,  
Sucharita Dutta<sup>3</sup>, Meredith R. Clark<sup>3</sup>, Gustavo F. Doncel<sup>3</sup> and  
John B. Cooper<sup>1\*</sup>

<sup>1</sup>Department of Chemistry and Biochemistry, Old Dominion University, Norfolk, VA, United States,

<sup>2</sup>Department of Physical and Macromolecular Chemistry, Charles University, Prague, Czechia, <sup>3</sup>CONRAD, Department of Obstetrics and Gynecology, Eastern Virginia Medical School, Norfolk, VA, United States

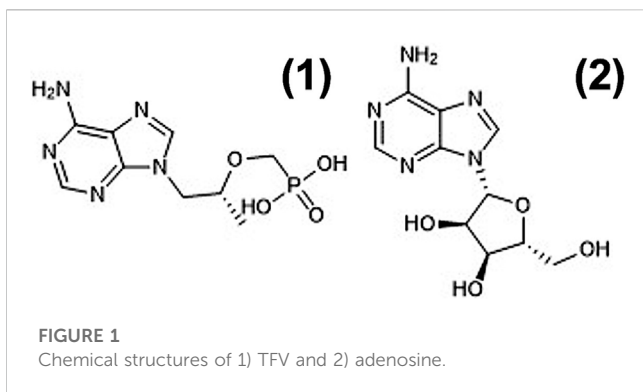
This study introduces a convenient and ultra-sensitive method of detection and quantification of the antiviral drug, tenofovir (TFV), by surface-enhanced Raman spectroscopy (SERS). Novel spatially resolved instrumentation for spectral acquisition and subsequent statistical analysis for hot spot selection was developed for convenient quantification of TFV in an aqueous matrix. Methods of statistical analysis include the use of partial least squares (PLS) regression vector analysis and spectral ranking by quality indices computed using CHAOS theory. Hydroxylamine-reduced Ag colloidal nanoparticles evaporated to dryness on an aluminum well-plate were used as the SERS substrate. To our knowledge, quantification of TFV down to 25 ng/mL by SERS, comprising clinically relevant concentrations, has not been previously reported. Furthermore, in this work we propose a novel method of quantification of aqueous TFV standards by SERS using statistical treatment of data by PLS and CHAOS theory. Based on these data, we propose future studies to develop a method of TFV detection and quantification in biological samples, beneficial to clinicians for rapid assessment of drug adherence during the treatment and prevention of viral diseases.

## KEYWORDS

surface-enhanced Raman spectroscopy (SERS), tenofovir (TFV), adenosine, Ag nanoparticles, pharmaceutical analysis, chemometrics

## 1 Introduction

Viral diseases are on the rise (Baker et al., 2022). Among them, human immunodeficiency virus (HIV) remains a prevalent infection, and according to UNAIDS, as of 2021, there were approximately 38.4 million individuals living with HIV worldwide, and about 1.3 million new infections per year. With HIV resources available totaling an estimated \$21.4 billion USD, it is estimated that 21.4 million individuals are accessing antiretroviral therapy and another 1.6 million are using these drugs for prevention of HIV (UNAIDS, 2022). Strict adherence to daily pill regimens is critical not only for the success of treatment and prevention of infection



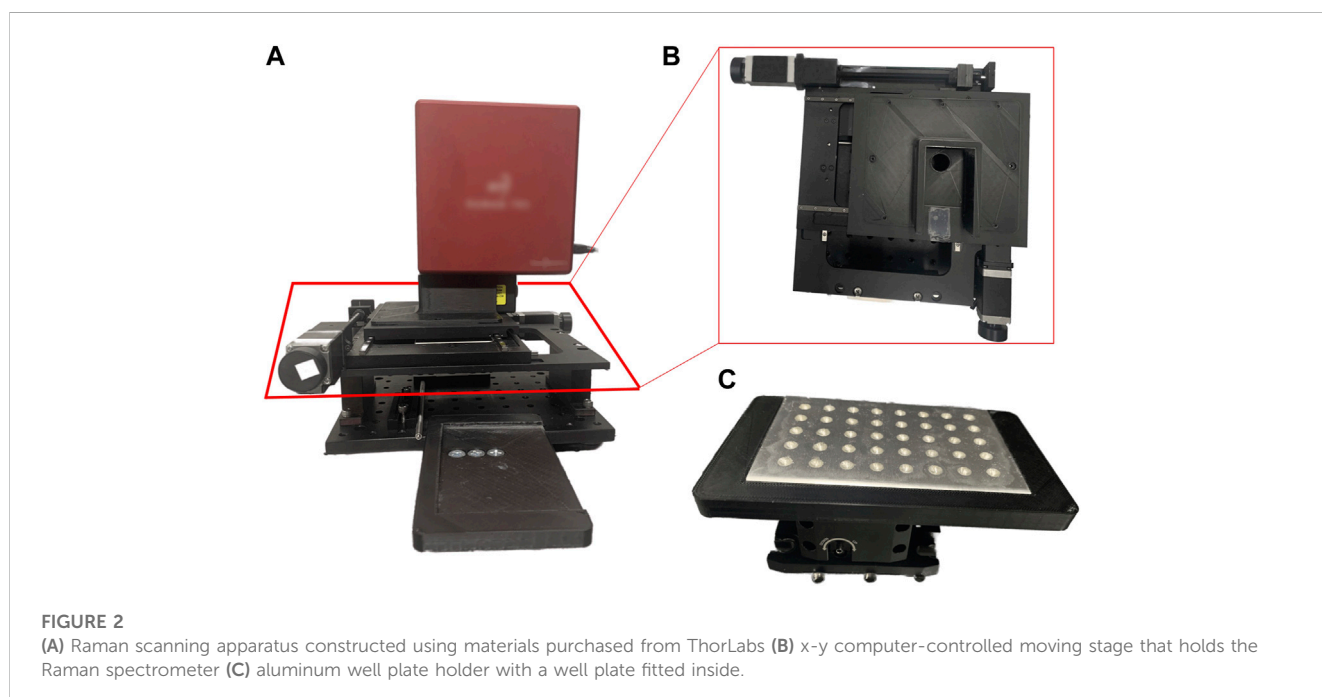
but also to avoid the emergence of drug resistance. Today, there is no commercially available point-of-care assay that may provide clinicians with objective evidence of the patients' drug adherence profile. Most of the assays used to quantify antiretroviral (ARV) drugs rely on liquid chromatography with tandem mass spectrometry (LC/MS/MS), an accurate but expensive and complex method that requires specialized

labs to be performed. Two lateral flow assays have been reported for the qualitative detection of tenofovir in urine (Hermans et al., 2023; McCluskey et al., 2023).

Among ARV drugs, tenofovir (TFV) is one widely used as part of the first-line therapeutic and preventive regimens (Venter et al., 2017). TFV is a synthetic acyclic nucleotide analogue of adenosine (see Figure 1) belonging to the medication class nucleoside reverse transcriptase inhibitors (NRTIs). TFV has a molecular formula of  $C_9H_{14}N_5O_4P$  and a molecular weight of 287.21 g/mol. TFV itself has poor oral bioavailability and is commonly administered in a prodrug form, tenofovir disoproxil fumarate (TDF) or tenofovir alafenamide fumarate (TAF). Briefly, following oral administration, TFV is activated via bi-phosphorylation and inhibits chain elongation by competing with deoxyadenosine 5'-triphosphate for chain incorporation during the synthesis of new viral DNA. When TFV is inserted in the chain in place of deoxyadenosine 5'-triphosphate, chain termination is induced, ultimately inhibiting viral DNA replication (National Center for Biotechnology Information, 2023). Tenofovir is used in the therapy of HIV and hepatitis B virus (HBV) infection (National Center for Biotechnology Information, 2023).

**TABLE 1** Instrument parameters used for acquisition of spatially-resolved SERS spectra.

Separation between wells ( $\mu\text{m}$ )	12,700	Time to scan a well (min)	24.08
Starting x position	13,000	Spatial Resolution ( $\mu\text{m}$ )	100
Starting y position	11,000	Spectral integration time (ms)	800
Well diameter scanned ( $\mu\text{m}$ )	6,000	Laser power	15 mW
Scan velocity ( $\mu\text{m}/\text{sec}$ )	124	Laser wavelength (nm)	785
Number of wells in row (moving X)	5	Number of spectra per well	1806
Number rows (moving Y)	8	Total spectra	72,240



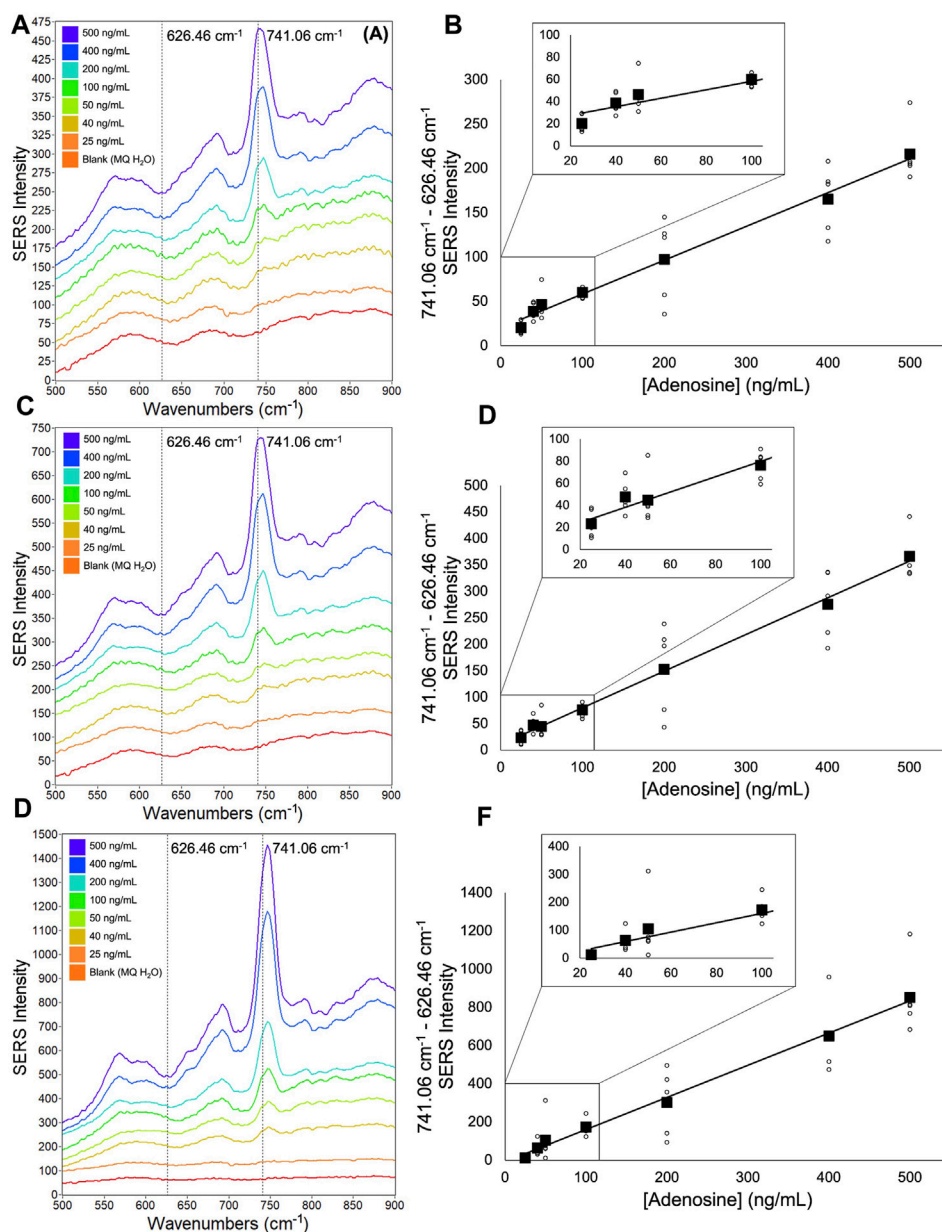


**FIGURE 3**

Averaged adenosine SERS spectra and corresponding calibration curves (A) 9,030 spectra (100% spectra) averaged per concentration (B) corresponding calibration curve (C) 4,515 spectra (50% spectra) averaged per concentration (D) corresponding calibration curve (E) 900 spectra (10% spectra) averaged per concentration (F) corresponding calibration curve. Calibration curves show the difference of SERS intensity between 626.46 cm<sup>-1</sup> and 741.06 cm<sup>-1</sup> plotted as a function of adenosine concentration. All spectra had a 5-point Savitzky-Golay (S-G) smoothing function applied and were offset for clarity. Zoomed insets of calibration curves magnify adenosine concentrations 25 ng/mL–100 ng/mL.

Surface-enhanced Raman spectroscopy (SERS) is a highly sensitive analytical method that utilizes surface plasmon resonances (SPR) from metal nanostructures for detection of molecules (Schlücker, 2009). Briefly summarizing the theory of SERS, incident photons from a laser beam colliding with a molecule will result in a perturbation of its electron distribution, causing geometric distortion. In response, regions of the molecule will generate an electric dipole moment. This relationship can be mathematically modeled in Eq. 1 such that the induced dipole

moment,  $\rho$ , is directly proportional to the electric field strength,  $E$  (Aroca and Rodriguez-Llorente, 2006).

$$\rho = \alpha E \quad (1)$$

Termed inelastic scattering, as the molecule undergoes an energy transition following a collision with incident photons, a small fraction of these photons will scatter at a different frequency than their initial frequency from the laser beam. Stokes and anti-Stokes shifts describe scattered photons whose vibrational energy is

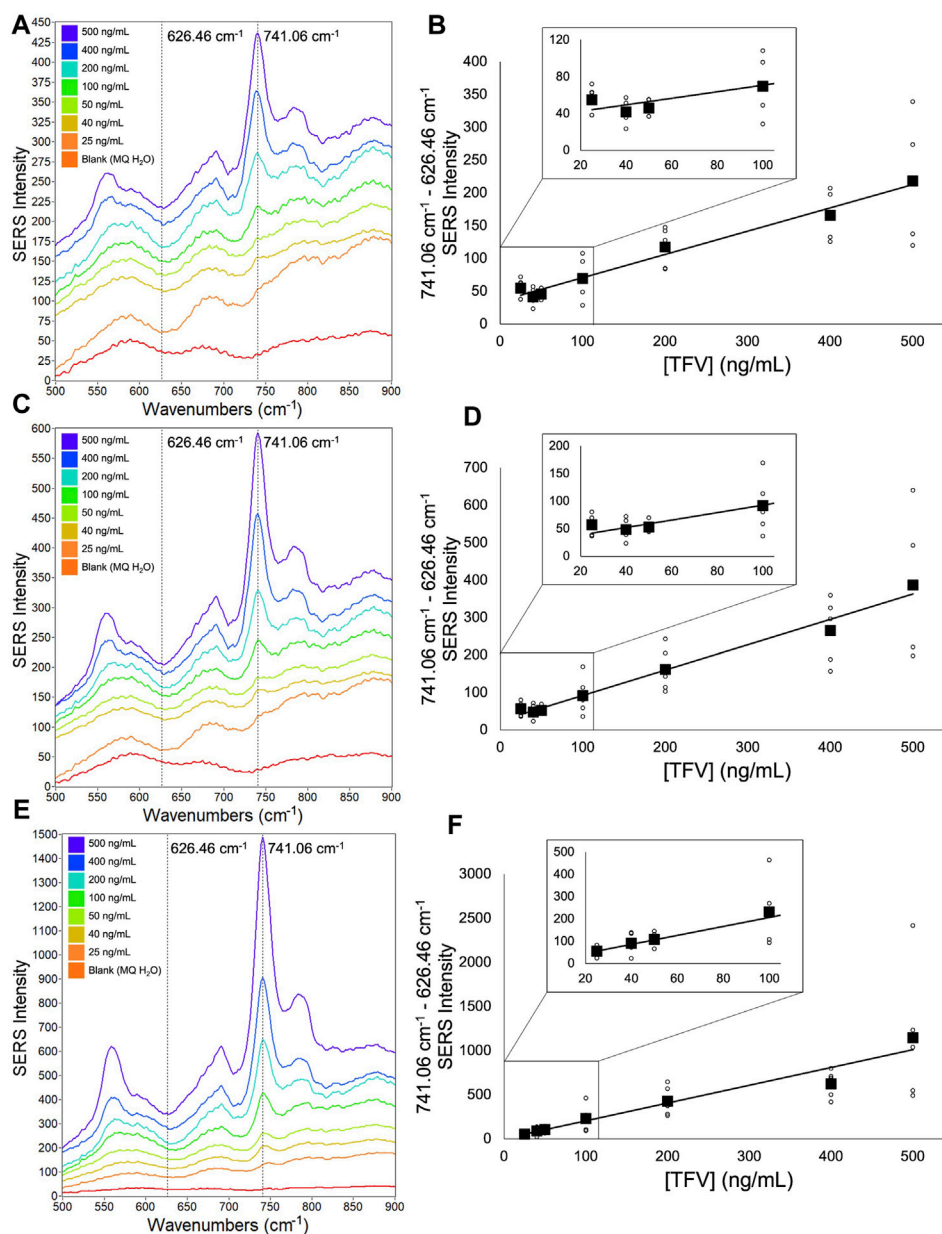


**FIGURE 4**

Averaged single-aliquot TFV SERS spectra and corresponding calibration curves (A) 9,030 spectra (100% spectra) averaged per concentration (B) corresponding calibration curve (C) 4,515 spectra (50% spectra) averaged per concentration (D) corresponding calibration curve (E) 900 spectra (10% spectra) averaged per concentration (F) corresponding calibration curve. Calibration curves show the difference of SERS intensity between 626.46 cm<sup>-1</sup> and 741.06 cm<sup>-1</sup> plotted as a function of TFV concentration. All spectra had a 5-point Savitzky-Golay (S-G) smoothing function applied and were offset for clarity. Zoomed insets of calibration curves magnify TFV concentrations 25 ng/mL–100 ng/mL.

higher or lower than their initial energy, respectively. Relevant factors that contribute to signal enhancement of Raman scattering, termed surface-enhanced Raman scattering (SERS), include the optical properties, light absorption, and scattering by metal nanoparticles (Schlücker, 2009). Additionally, SERS is dependent on the optical phenomenon surface plasmon resonance (SPR). Briefly, SPR provides electric enhancement on the nanostructure surface. When a metal nanostructure experiences an electric field from incident polarized light, polarization of the electron cloud surrounding the nanostructure occurs, resulting in charge separation (Jana et al., 2016). At a particular angle of this

interaction (the angle of incidence), photon energy will couple with electrons on the metal surface, resulting in changes in the atomic nuclear coordinates (Nguyen et al., 2015). Surface plasmons can be excited in small metal particles or a metal-containing non-uniform surface. The morphology of these metal nanostructures, including size, shape, and composition, has been reported extensively in literature as a factor of SERS enhancement and SPR (Fleger and Rosenbluh, 2009). The morphology and size of Ag nanoparticles can influence SERS enhancement. Silver nanostructures of different shapes have different plasmon modes (Puente et al., 2023), and thus will exhibit different levels of electromagnetic enhancement

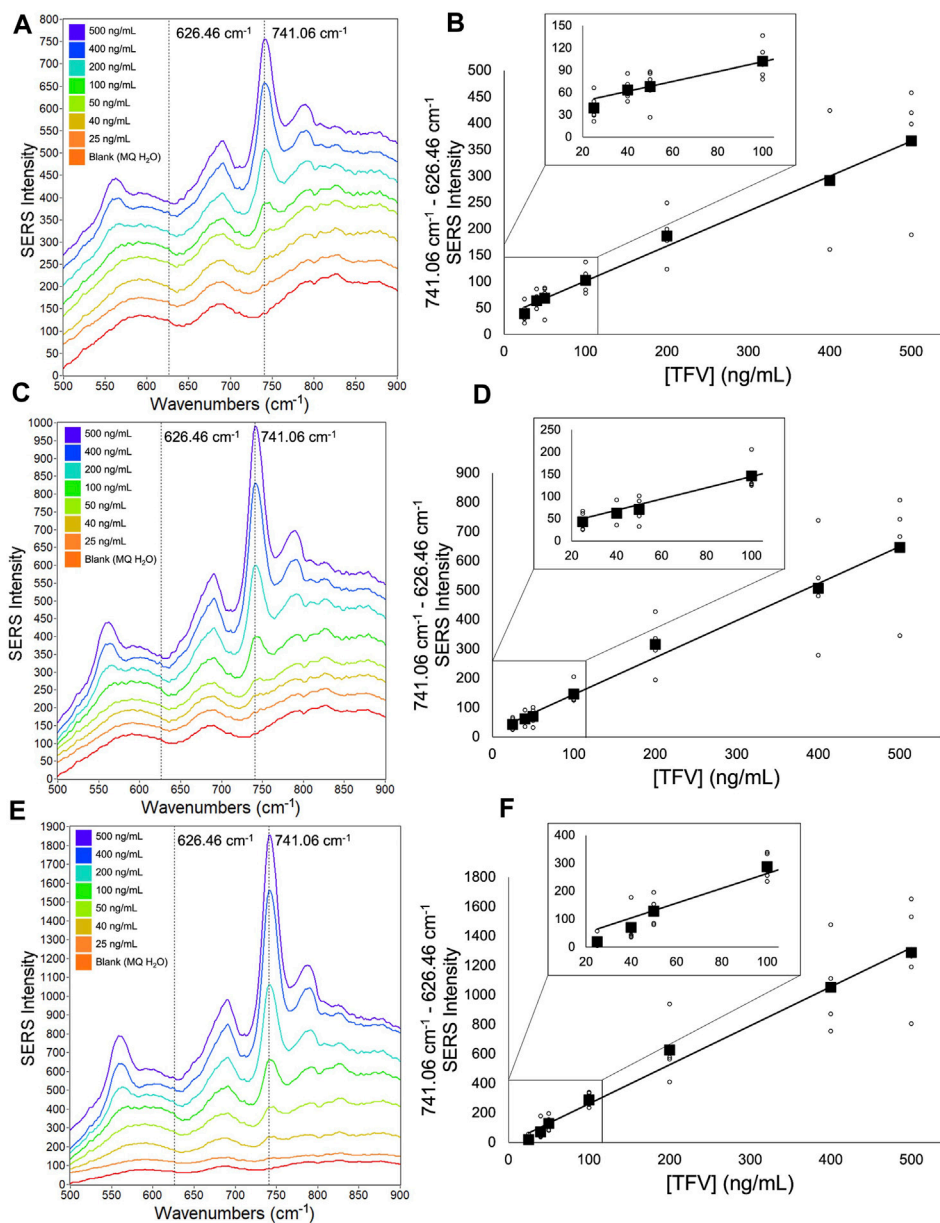


**FIGURE 5**

Averaged double-aliquot TFV SERS spectra and corresponding calibration curves (A) 9,030 spectra (100% spectra) averaged per concentration (B) corresponding calibration curve (C) 4,515 spectra (50% spectra) averaged per concentration (D) corresponding calibration curve (E) 900 spectra (10% spectra) averaged per concentration (F) corresponding calibration curve. Calibration curves show the difference of SERS intensity between 626.46  $\text{cm}^{-1}$  and 741.06  $\text{cm}^{-1}$  plotted as a function of TFV concentration. All spectra had a 5-point Savitzsky-Golay (S-G) smoothing function applied and were offset for clarity. Zoomed insets of calibration curves magnify TFV concentrations 25 ng/mL–100 ng/mL.

**TABLE 2** Correlation coefficient, linear slope, and y-intercept values for calibration curves of adenosine data shown in Figure 3.

Calibration curve	$R^2$	Linear slope	y- intercept
Figure 3B	0.9926	0.3814	20.117
Figure 3D	0.9966	0.6938	10.532
Figure 3F	0.9956	1.6859	-8.3682

**TABLE 3** Correlation coefficient, linear slope, and y-intercept values for calibration curves of TFV single-aliquot data shown in Figure 4.

Calibration curve	$R^2$	Linear slope	y- intercept
Figure 4B	0.9816	0.3552	35.274
Figure 4D	0.9829	0.6765	25.035
Figure 4F	0.9421	2.0109	5.6613

**TABLE 4** Correlation coefficient, linear slope, and y-intercept values for calibration curves of TFV double-aliquot data shown in Figure 5.

Calibration curve	$R^2$	Linear slope	y- intercept
Figure 5B	0.9939	0.6628	35.139
Figure 5D	0.9930	1.2619	18.744
Figure 5F	0.9906	2.6474	-1.3667

relative to each other. Different capping agents (i.e., chloride ions, citrate, polyvinylpyrrolidone, etc.) used for aggregation control of nanoparticle suspensions also influences the resulting size and shape of the nanoparticles (Javed et al., 2020; Yang et al., 2020).

SERS has emerged as a highly sensitive technique for detecting drugs by generating unique vibrational spectra for specific molecules (Thobakgale et al., 2022). This approach offers a considerable advantage over conventional methods such as LC-MS/MS, which involve complex instrumentation and sample preparation (Lin et al., 2023). Other methods of detection of aqueous TFV include square-wave voltammetry where Festinger and coworkers reported limits of detection as low as  $1.35 \times 10^{-7}$  M (39 ng/mL) and  $4.86 \times 10^{-8}$  M (14 ng/mL) (Festinger et al., 2022). Chiral separation phase (CSP) LCMS of enantiomeric mixtures of a prodrug form of tenofovir, tenofovir disoproxil fumarate (TDF), reported limits of detection of 1.5 ng/mL and 1.2 ng/mL for the R- and S- TDF enantiomers, respectively (Lin et al., 2023). While these are very impressive limits of detection, these methods require complex instrumentation and skill. In this paper, detection of TFV down to 25 ng/mL was achieved using SERS. Analysis by SERS can also be applied to field studies whereas LC- MS/MS requires vacuum technology and expensive detectors for accurate mass measurements as well as considerable operator skills. The SERS platform itself is also considerably smaller than LC- MS/MS apparatuses. Nevertheless, it should be noted that the reaction mixture of a 1:1 solution of Ag colloidal nanoparticles and aqueous TFV used in this study inherently dilutes the TFV present in the reaction mixture, potentially limiting detection and quantification limits. However, evaporating the reaction mixture to dryness significantly enhances the quantifiable detection limit by effectively concentrating the reaction mixture through evaporation of the solvent. This deposition technique allows multiple depositions due to the lack of spatial constraints that exist in a liquid-phase reaction mixture. In this study, a double-deposition TFV experiment is presented, which demonstrates improved spectral signal-to-noise ratio (S/N) and linearity of quantitation compared to a single-deposition experiment. Statistical variability with respect to SERS enhancement and quantification was also considered in the interpretation of results. To overcome this, a variety of statistical treatments were applied to large data sets to generate reproducible quantitative data. We aim to apply these results and methods of analysis to clinical samples for quantification of TFV and other HIV drug levels.

## 2 Materials and methods

### 2.1 Synthesis of Ag colloidal nanoparticles

Ag colloidal nanoparticles (CNP) were prepared by reduction of  $\text{AgNO}_3$  (Sigma- Aldrich,  $\geq 99.0\%$ ) with  $\text{NH}_2\text{OHHCl}$  (Sigma) as

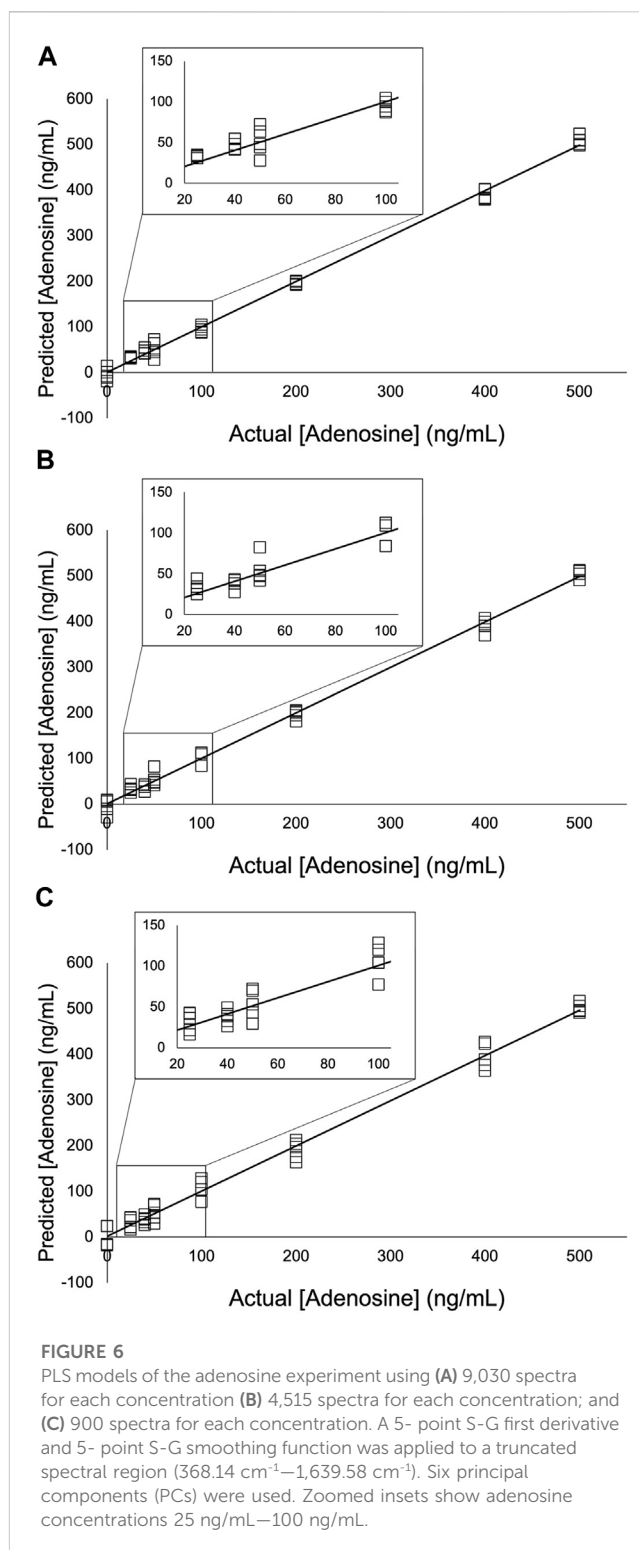


**FIGURE 6** PLS models of the adenosine experiment using (A) 9,030 spectra for each concentration (B) 4,515 spectra for each concentration; and (C) 900 spectra for each concentration. A 5- point S-G first derivative and 5- point S-G smoothing function was applied to a truncated spectral region ( $368.14 \text{ cm}^{-1}$ – $1,639.58 \text{ cm}^{-1}$ ). Six principal components (PCs) were used. Zoomed insets show adenosine concentrations 25 ng/mL–100 ng/mL.

described by Leopold and Lendl (Leopold and Lendl, 2003). Briefly, a 90 mL  $\text{NH}_2\text{OHHCl}$  solution with a concentration of  $1.6 \times 10^{-3}$  M was prepared. 300  $\mu\text{L}$  of 1 M NaOH (Fisher Chemical) was then added to this solution. The solution was stirred continuously at 350 rpm as 10 mL of  $1 \times 10^{-2}$  M  $\text{AgNO}_3$  was added dropwise to the solution. The solution was stirred for an additional 45 min. See Supplementary Figure S1 for UV- Vis spectra of CNP syntheses used in this study. Dynamic light scattering (DLS) of a prepared silver

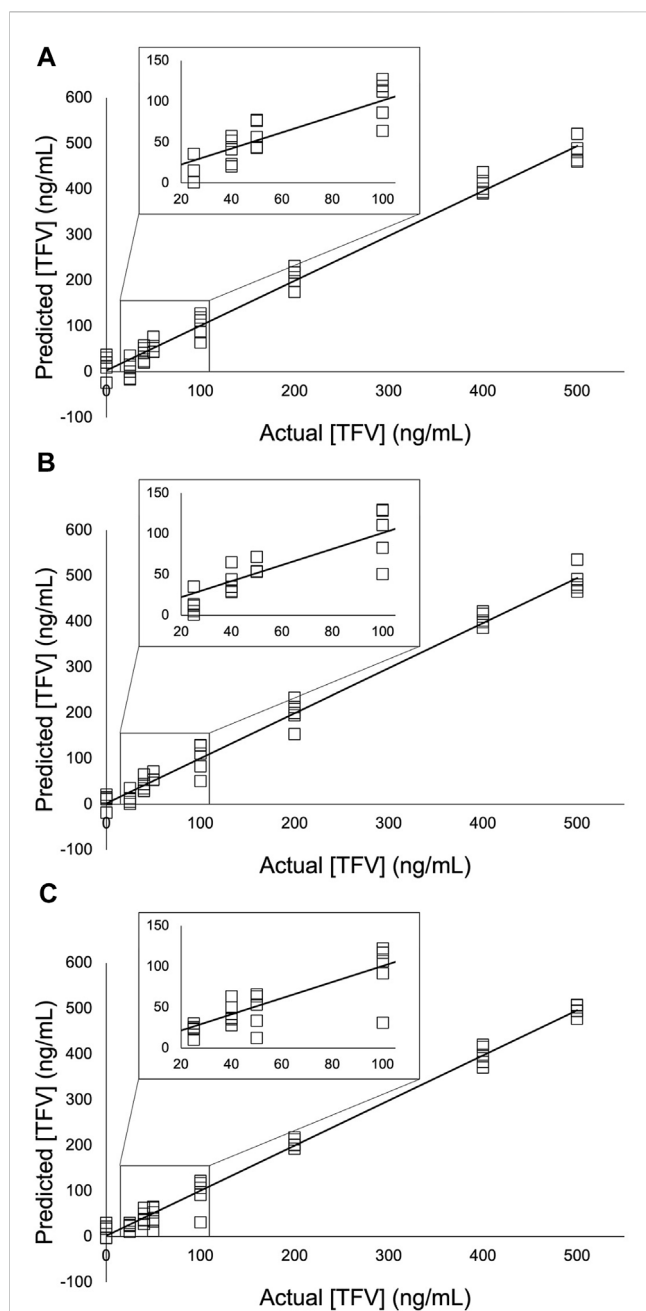


**FIGURE 7**

PLS models of the TFV single-aliquot experiment using (A) 9,030 spectra for each concentration (B) 4,515 spectra for each concentration; and (C) 900 spectra for each concentration. A 3-point S-G first derivative and 5-point S-G smoothing function was applied to a truncated spectral region ( $368.14\text{ cm}^{-1}$ – $1,072.6\text{ cm}^{-1}$ ). Six principal components (PCs) were used. Zoomed insets show TFV concentrations 25 ng/mL–100 ng/mL.

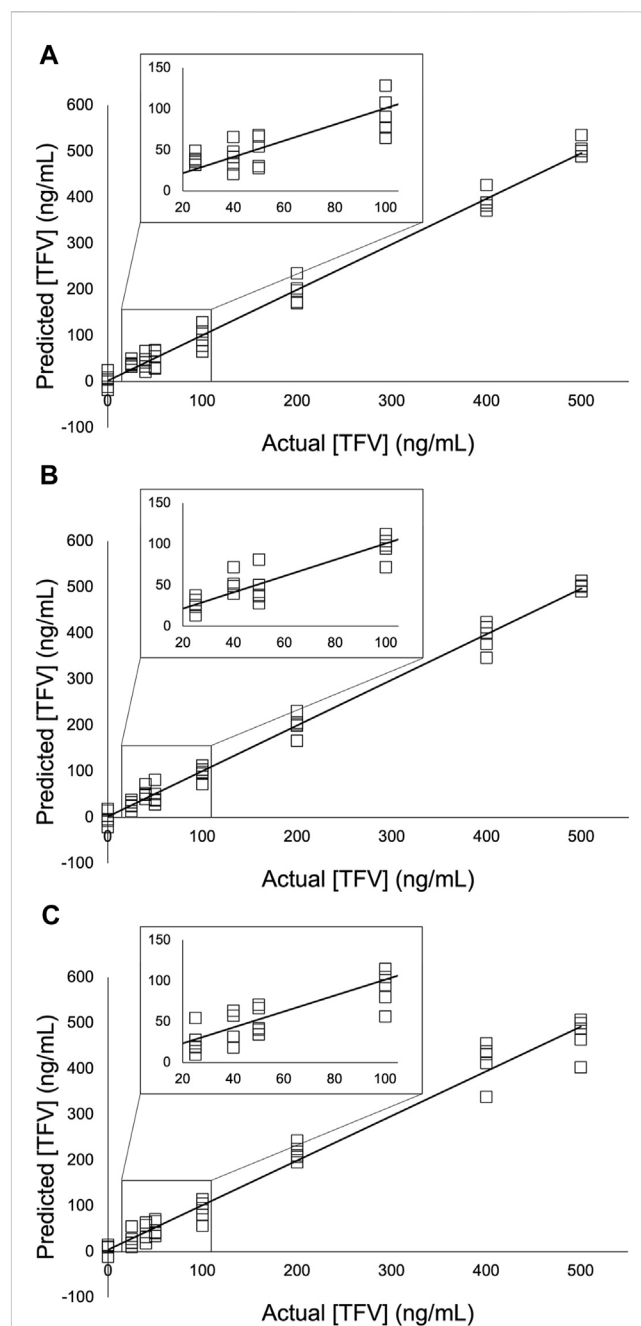


**FIGURE 8**

PLS models of the TFV double-aliquot experiment using (A) 9,030 spectra for each concentration (B) 4,515 spectra for each concentration; and (C) 900 spectra for each concentration. A 5-point S-G first derivative and 7-point S-G smoothing function was applied to a truncated spectral region ( $368.14\text{ cm}^{-1}$ – $1,639.58\text{ cm}^{-1}$ ). Five principal components (PCs) were used. Zoomed insets show TFV concentrations 25 ng/mL–100 ng/mL.

colloidal suspension following our experimental conditions was performed using a NanoBrook particle analyzer (Brookhaven). The average effective particle diameter was measured to be 56.42 nm with an average polydispersity index of 0.312. See [Supplementary Figure S2](#) and [Supplementary Table S1](#) for the differential distribution of particle diameter, instrument parameters, and summary statistics.

## 2.2 Preparation of TFV and adenosine standards for spectra acquisition

Powder TFV and adenosine were provided by CONRAD at Eastern Virginia Medical School and manufactured by Gilead Alberta ULC. Serial dilutions from an aqueous stock of 100  $\mu\text{g}/$

**TABLE 5** Correlation coefficient, linear slope, and y-intercept values for calibration curves of adenosine data shown in [Figure 6](#).

Calibration curve	$R^2$	Linear slope	y- intercept
<a href="#">Figure 6A</a>	0.9960	0.9960	0.6574
<a href="#">Figure 6B</a>	0.9951	0.9951	0.7976
<a href="#">Figure 6C</a>	0.9903	0.9903	1.5948

**TABLE 6** Correlation coefficient, linear slope, and y-intercept values for calibration curves of TFV single-aliquot data shown in [Figure 7](#).

Calibration curve	$R^2$	Linear slope	y- intercept
<a href="#">Figure 7A</a>	0.9833	0.9833	2.7529
<a href="#">Figure 7B</a>	0.9863	0.9863	2.2528
<a href="#">Figure 7C</a>	0.9891	0.9891	1.7954

**TABLE 7** Correlation coefficient, linear slope, and y-intercept values for calibration curves of TFV double-aliquot data shown in [Figure 8](#).

Calibration curve	$R^2$	Linear slope	y- intercept
<a href="#">Figure 8A</a>	0.9886	0.9886	1.8689
<a href="#">Figure 8B</a>	0.9903	0.9903	1.5904
<a href="#">Figure 8C</a>	0.9758	0.9758	3.9843

mL TFV and adenosine were performed for subsequent concentration gradients. An aluminum plate containing 40 machined wells in an  $8 \times 5$  well-plate, each having a volume capacity of  $20 \mu\text{L}$ , was used as our SERS surface. Certified 1,100 aluminum was used for the well plate construction. In between experiment replicates, the plate was cleaned by soaking in a 1 M NaOH bath and hand milling with a drill bit, followed by deposition of 4 M  $\text{HClO}_4$  into the wells and thorough DI  $\text{H}_2\text{O}$  rinsing.

All samples presented in this study underwent the preparation and spectra acquisition parameters described in the preceding section. A 1:1 mixture of Ag CNP and analyte was prepared in a microcentrifuge tube and vortexed for 5 seconds.  $20 \mu\text{L}$  aliquots of this mixture were added into each well where each TFV concentration was deposited into five aluminum wells and taken to dryness in a chemical hood prior to spectra acquisition. Since the evaporative process is stochastic, the total volume for all reaction mixtures remained constant (i.e., equivalent volumes of CNP suspension and aqueous TFV or adenosine standards, where each standard is a different concentration). For the TFV double-aliquot experiment, this mixture, deposition, and evaporation process was repeated for one additional aliquot of  $20 \mu\text{L}$  in each well. A high-resolution “square” scan was acquired of each well in the well plate following parameters described in [Table 1](#). The platform by which statistical analysis is performed was developed by our group at Old Dominion University. A computerized XY stage (ThorLabs) holding the Wasatch Photonics 785 nm Raman spectrometer (Kent Lawson Wise and Lee Schoen, 2002) was used for automated spectra acquisition of each well in the aluminum well plate. A raster scan pattern was used for acquisition. See [Figure 2](#) for images of the

sampling apparatus. Additional acquisition software setup parameters are listed in [Supplementary Figure S3](#).

## 3 Results and discussion

### 3.1 Quality indexing of acquired spectra

For all experiments, 1806 spectra were acquired of each sample well. Statistical analysis was done on acquired spectra to generate calibration curves of TFV and adenosine. Adenosine was investigated in this study for the purpose of comparison with TFV analysis (see [Figure 3](#); [Figure 4](#)) because the adenine ring-breathing peak was used for quantification of both analytes and TFV’s inherent derivation from adenosine. See [Supplementary Figure S7](#) and [Supplementary Table S2](#) for peak assignments from acquired TFV data compared to literature assignments. Calibration curves were also generated for the double aliquot TFV experiment (see [Figure 5](#)) to probe the benefit of evaporating our reaction mixture of TFV and CNP to dryness then depositing an additional aliquot. Spectra were statistically analyzed using quality indexes ( $Q_i$ ) calculated from the intensity of the adenine ring-breathing peak in the spectral region  $739\text{--}745 \text{ cm}^{-1}$ .

The calculation of spectra quality indexes in general terms is described in the preceding paragraph. The subscript indexes, positions of cursors in the data processing program, p: peak;  $b_1$ : baseline 1;  $b_2$ : baseline 2. Baselines are defined in [Eqs 2, 3](#).

$$b_1 = p - 2(\text{FWHM}) \quad (2)$$

$$b_2 = p + 2(\text{FWHM}) \quad (3)$$

Where FWHM is defined as the full width and half max of the selected peak(s) of interest. To maximize S/N of the selected peak(s) of interest, a summation of intensities at respective points, generally defined as point j,  $I_j$ , can be calculated to determine the average intensity about each peak at a user-defined range of points to the right of the selected cursor. The difference between these intensity summations with respect to peak(s) and their respective baselines are defined as a quality index ( $Q_i$ ) used for spectral ranking in this study, defined in [Eq. 4](#).

$$Q_i = \left[ \prod_{k=1}^{k=t} \left[ \frac{1}{2n+1} \left[ \left( \sum_{j=p-n}^{p+n} I_j - \sum_{j=b_1-n}^{b_1+n} I_j \right) \times \left( \sum_{j=p-n}^{p+n} I_j - \sum_{j=b_2-n}^{b_2+n} I_j \right) \right] \right] \right]_k \quad (4)$$

$$\{Q_i < 0 \neq Q_i = 0\}$$

Where t is defined as the total number of peaks factored into the  $Q_i$ . The  $Q_i$  value is also conditional such that any calculated  $Q_i$  less than 0 is equal to 0, defined in [Eq. 5](#). [Supplementary Figures S4–S6](#) show scatter diagrams of all spectra  $Q_i$  values corresponding to each concentration for these experiment sets. All  $Q_i$  data corresponding to acquired spectra was then written into a new file and uploaded to a second data processing program.

The second data processing program employed a selection criterion that involved choosing a percentage of high-quality spectra prior to computing an average spectrum for each well. Each averaged spectrum corresponding to the same concentration, a total of five each because each concentration had five replicates, were then averaged, generating a single averaged spectrum for each concentration. This selection process



was carried out based on the  $Q_i$  values computed in the first data processing program, allowing the second data processing program to sort the  $Q_i$  values for each well. The selected percentages of spectra from each well factored into the total averaged spectrum for each concentration was comprised of spectra corresponding to the highest  $Q_i$  values within that percent range. Using this program, three different percentages of spectra acquired for each replicate were averaged (Figures 3–5): 100% (1806 spectra), 50% (903 spectra), and 10% (180 spectra) and used for analysis in the preceding section. SERS Enhancement factors (EFs) were calculated for each dataset and are shown in Supplementary Table S3. Briefly, for each concentration, the spectrum corresponding to the maximum SERS intensity of the  $741\text{ cm}^{-1}$  peak was divided by the average  $741\text{ cm}^{-1}$  peak intensity for all spectra. These quotients were then multiplied by  $10^6$ , an established EF of a prominent adenine peak ( $733\text{--}740\text{ cm}^{-1}$ ) (Sivaprakasam and Hart, 2021). From these calculations, our system of Ag CNP and analyte mixtures evaporated to dryness exhibited relative EFs between  $10^7$  and  $10^6$  across all concentrations.

### 3.2 Calibrations of experiment sets

For all three experiment sets, based on the analysis of the three percentage subsets of spectra above, using 50% of spectra (903 spectra) from each well for each concentration yielded linear correlations similar to that using 100% of the spectra for each well for each concentration (Table 2; Table 3; Table 4). However, the 50% spectral subsets showed increased S/N in the total averaged spectra compared to the 100% spectral subsets. The 10% spectral subsets generated averaged spectra with the highest S/N, however the smaller sampling size drastically increased the standard deviation and decreased the linearity across the three sample sets. Based on this result, 50% spectral subsets appeared to be the most representative of the entire data population corresponding to each concentration yet also sufficiently excluded spectra with low quality indexes and poor S/N with respect to the adenine ring-breathing peak in the  $739\text{--}745\text{ cm}^{-1}$  region. Limits of detection for all experiment sets were calculated by averaging the S/N for each TFV concentration and are shown in Supplementary Table S4.

A notable aspect of our analysis was investigating the impact of a second aliquot of the TFV and Ag CNP mixture after the initial aliquot was taken to dryness versus a single aliquot of the TFV and Ag CNP mixture with respect to spectra signal enhancement, analytical sensitivity, and the ability to differentiate between TFV concentrations 25 ng/mL, 40 ng/mL, and 50 ng/mL. From data presented in Figure 4 and Figure 5, it was shown that the double-aliquot TFV experiment exhibited superior signal-to-noise ratios in the averaged concentration spectra to the single-aliquot TFV averaged concentration spectra. Additionally, the double-aliquot TFV experiment demonstrated improved linearity in the concentration calibration curve with respect to the correlation coefficient, coinciding with improved discrimination between concentrations 25 ng/mL, 40 ng/mL, and 50 ng/mL. Furthermore, double-aliquot calibrations demonstrated higher analytical sensitivity across all subsets than single-aliquot calibrations as shown by the higher slope values (Tables 3, 4). This result is consistent with the benefit of our sampling apparatus such that evaporating the analyte and Ag CNP reaction mixture to dryness

has a concentrating effect on the analyte of interest, and a second aliquot of the mixture taken to dryness enhances the SERS signal of our analyte even more, possibly from the increased amount of TFV detected at the sensitivity of the system. In addition to the improved distinction between 25 ng/mL, 40 ng/mL, and 50 ng/mL, these results suggest that with a second reaction mixture aliquot, there is better analyte/CNP well coverage, resulting in a greater amount of high  $Q_i$  spectra, highlighting another benefit of our sampling apparatus. In addition, the standard deviation for each concentration in the calibration curves also improved for the double aliquot experiments compared to the single aliquot experiments (see Supplementary Tables S5–S7). The standard deviation of the 40 ng/mL and 50 ng/mL data points were closer in value to each other in the double aliquot experiment, compared to the single aliquot experiment where the standard deviation of the 40 ng/mL data point was nearly double the standard deviation of 50 ng/mL. This is also observed between the 500 ng/mL and 400 ng/mL data points, where they are close in value in the double aliquot experiment, but the 500 ng/mL standard deviation is nearly double the 400 ng/mL standard deviation in the single-aliquot experiment. This improvement in both analytical sensitivity and precision suggests that the additional aliquot provides better well coverage and an increase in hot spots for sample wells.

### 3.3 Partial least squares regression analysis of experiment sets

Partial least squares (PLS) regression analysis was applied to the three experiments presented in this study (Figure 6; Figure 7; Figure 8). The collinear nature of each factor modeled by these regressions was used to predict responses of future factors with respect to these models whose TFV concentrations are unknown. Correlation coefficient, slope, and y-intercept values for these regressions are shown in Table 5, Table 6, and Table 7. Extending these findings into future work, our aim is to use these analytical methods of TFV and apply them to analysis of TFV in biological samples for detection and quantification. This is currently under investigation by our group.

## 4 Conclusion

In conclusion, this study demonstrated detection and quantification of the antiviral HIV drug tenofovir using surface-enhanced Raman spectroscopy down to 25 ng/mL. This was achieved using hydroxylamine-reduced Ag colloidal nanoparticles as the SERS substrate and novel acquisition and processing software for spectra acquisition and statistical analysis. An  $8 \times 5$  aluminum well plate with machined wells was used as the SERS surface. The statistical methods used, including partial least squares (PLS) regression and spectra ranking by quality indices computed using CHAOS theory, proved to be effective in the quantification of TFV in an aqueous matrix. These data show promise for future studies aimed at detecting and quantifying TFV in biological samples by SERS, which could provide clinicians with a rapid and convenient means of objectively assessing drug adherence in the treatment and prevention of viral diseases such as HIV.

## Data availability statement

The original contributions presented in the study are included in the article/Supplementary Materials, further inquiries can be directed to the corresponding author.

## Author contributions

MB: Conceptualization, Data curation, Formal Analysis, Investigation, Methodology, Validation, Writing—original draft, Writing—review and editing. JH: Conceptualization, Methodology, Resources, Validation, Writing—review and editing. TJ: Funding acquisition, Project administration, Supervision, Writing—review and editing. SD: Project administration, Supervision, Writing—review and editing. MC: Funding acquisition, Project administration, Supervision, Writing—review and editing, Conceptualization. GD: Funding acquisition, Project administration, Supervision, Writing—review and editing. JC: Funding acquisition, Project administration, Resources, Software, Supervision, Validation, Writing—review and editing, Conceptualization.

## Funding

The author(s) declare financial support was received for the research, authorship, and/or publication of this article. This work was funded by subaward ENS-20-001 from CONRAD/EVMS under Project Engage, a cooperative agreement (7200AA20CA00030) between the U.S. Agency for International Development (USAID)

## References

- Aroca, R. F., and Rodriguez-Llorente, S. (2006). *Surface enhanced vibrational spectroscopy*. Hoboken, New Jersey, United States: Wiley.
- Baker, R. E., Mahmud, A. S., Miller, I. F., Rajeev, M., Rasambainarivo, F., Rice, B. L., et al. (2022). Infectious disease in an era of global change. *Nat. Rev. Microbiol.* 20 (4), 193–205. doi:10.1038/s41579-021-00639-z
- Festinger, N., Spilarewicz-Stanek, K., Borowczyk, K., Guziejewski, D., and Smarzewska, S. (2022). Highly sensitive determination of tenofovir in pharmaceutical formulations and patients urine-comparative electroanalytical studies using different sensing methods. *Molecules* 27 (6), 1992. doi:10.3390/molecules27061992
- Fleger, Y., and Rosenbluh, M. (2009). Surface plasmons and surface enhanced Raman spectra of aggregated and alloyed gold-silver nanoparticles. *Res. Lett. Opt.* 2009, 475941–475945. doi:10.1155/2009/475941
- Hermans, L. E., Umunnakwe, C. N., Lalla-Edward, S. T., Hebel, S. K., Tempelman, H. A., Nijhuis, M., et al. (2023). Point-of-Care tenofovir urine testing for the prediction of treatment failure and drug resistance during initial treatment for human immunodeficiency virus type 1 (HIV-1) infection. *Clin. Infect. Dis.* 76 (3), e553–e560. doi:10.1093/cid/ciac755
- Jana, J., Ganguly, M., and Pal, T. (2016). Enlightening surface plasmon resonance effect of metal nanoparticles for practical spectroscopic application. *RSC Adv.* 6 (89), 86174–86211. doi:10.1039/C6RA14173K
- Javed, R., Zia, M., Naz, S., Aisida, S. O., Ain, N. u., and Ao, Q. (2020). Role of capping agents in the application of nanoparticles in biomedicine and environmental remediation: recent trends and future prospects. *J. Nanobiotechnology* 18 (1), 172. doi:10.1186/s12951-020-00704-4
- Kent Lawson Wise, J. B. C., and Lee Schoen, C. (2002). Dispersive near-ir Raman spectrometer. *U. S. Pat. Appl.*
- Leopold, N., and Lendl, B. (2003). A new method for fast preparation of highly surface-enhanced Raman scattering (SERS) active silver colloids at room temperature by reduction of silver nitrate with hydroxylamine hydrochloride. *J. Phys. Chem. B* 107 (24), 5723–5727. doi:10.1021/jp027460u
- Lin, L., Huang, L., Ke, Y., Xu, X., and Huang, L. (2023). Study on quality control of tenofovir disoproxil fumarate enantiomers by high-performance liquid

and EVMS funded by U.S. President's Emergency Plan for AIDS Relief (PEPFAR). The views of the authors do not necessarily reflect those of the funding agency, PEPFAR or the US Government.

## Conflict of interest

The authors declare that the research was conducted in the absence of any commercial or financial relationships that could be construed as a potential conflict of interest.

The author(s) declared that they were an editorial board member of Frontiers, at the time of submission. This had no impact on the peer review process and the final decision.

## Publisher's note

All claims expressed in this article are solely those of the authors and do not necessarily represent those of their affiliated organizations, or those of the publisher, the editors and the reviewers. Any product that may be evaluated in this article, or claim that may be made by its manufacturer, is not guaranteed or endorsed by the publisher.

## Supplementary material

The Supplementary Material for this article can be found online at: <https://www.frontiersin.org/articles/10.3389/fnano.2023.1270474/full#supplementary-material>

chromatography–mass spectrometry. *Chromatographia* 86 (3), 213–222. doi:10.1007/s10337-023-04240-9

McCluskey, S. M., Govender, K., Adamson, J., Gandhi, M., Spinelli, M. A., Moosa, M.-Y., et al. (2023). Point-of-care urine tenofovir testing to predict HIV drug resistance among individuals with virologic failure. *AIDS Lond. Engl.* 37 (7), 1109–1113. doi:10.1097/qad.0000000000003520

National Center for Biotechnology Information, 2023 PubChem compound summary for CID 464205, tenofovir. Available: <https://pubchem.ncbi.nlm.nih.gov/compound/Tenofovir>.

Nguyen, H., Park, J., Kang, S., and Kim, M. (2015). Surface plasmon resonance: A versatile technique for biosensor applications. *Sensors* 15 (5), 10481–10510. doi:10.3390/s150510481

Puente, C., Pineda Aguilar, N., Gómez, I., and López, I. (2023). Morphology effect of photoconverted silver nanoparticles on the performance of surface-enhanced Raman spectroscopy substrates. *ACS Omega* 8 (14), 12630–12635. doi:10.1021/acsomega.2c05958

Schlücker, S. (2009). SERS microscopy: nanoparticle probes and biomedical applications. *Chemphyschem* 10 (9-10), 1344–1354. doi:10.1002/cphc.200900119

Sivaprakasam, V., and Hart, M. B. (2021). Surface-enhanced Raman spectroscopy for environmental monitoring of aerosols. *ACS Omega* 6 (15), 10150–10159. doi:10.1021/acsomega.1c00207

Thobakgale, S. L., Ombinda-Lemboumba, S., and Mthunzi-Kufa, P. (2022). A molecular study of Aspirin and tenofovir using gold/dextran Nanocomposites and surface-enhanced Raman spectroscopy. *Molecules* 27 (8), 2554. doi:10.3390/molecules27082554

UNAIDS (2022). *Danger: UNAIDS global AIDS update 2022*. Geneva, Switzerland: Joint United Nations Programme on HIV/AIDS.

Venter, W. D. F., Clayden, P., and Serenata, C. (2017). The ADVANCE study: A groundbreaking trial to evaluate a candidate universal antiretroviral regimen. *Curr. Opin. HIV AIDS* 12 (4), 351–354. doi:10.1097/coh.0000000000000389

Yang, T.-H., Shi, Y., Janssen, A., and Xia, Y. (2020). Surface capping agents and their roles in shape-controlled synthesis of colloidal metal nanocrystals. *Angew. Chem. Int. Ed.* 59 (36), 15378–15401. doi:10.1002/anie.201911135